Sn doped β–Ga_2O_3 and β–Ga_2S_3 nanowires with red emission for solar energy spectral shifting

M. Zervos' , A. Othonos, V. Gianneta, A. Travlos, and A. G. Nassiopoulou

Citation: Journal of Applied Physics **118**, 194302 (2015); doi: 10.1063/1.4935633
View online: http://dx.doi.org/10.1063/1.4935633
View Table of Contents: http://aip.scitation.org/toc/jap/118/19
Published by the American Institute of Physics

JOURNAL OF APPLIED PHYSICS **118**, 194302 (2015)

Sn doped β-Ga_2O_3 and β-Ga_2S_3 nanowires with red emission for solar energy spectral shifting

M. Zervos,[1,a)] A. Othonos,[2] V. Gianneta,[3] A. Travlos,[3] and A. G. Nassiopoulou[3]
[1]*Nanostructured Materials and Devices Laboratory, Department of Mechanical and Manufacturing Engineering, University of Cyprus, P.O. Box 20537, Nicosia 1678, Cyprus*
[2]*Laboratory of Ultrafast Science, Department of Physics, University of Cyprus, P.O. Box 20537, Nicosia 1678, Cyprus*
[3]*NCSR Demokritos, Institute of Nanoscience and Nanotechnology, 153 10 Aghia Paraskevi, Athens, Greece*

(Received 20 May 2015; accepted 1 November 2015; published online 17 November 2015)

Sn doped β-Ga_2O_3 nanowires have been grown on Si(001) via the vapor–liquid–solid mechanism at 800 °C over a broad range of compositions. These have a monoclinic β-Ga_2O_3 crystal structure and minimum resistances for 1–2 at. % Sn but we observe the emergence of tetragonal rutile SnO_2 which dominates with increasing content of Sn. All of the nanowires exhibited photoluminescence at 2.7 eV but a red shift of the emission occurred from 2.7 eV to 1.8 eV after post growth processing under H_2S above 500 °C. The red emission is related to deep donor to acceptor transitions and the formation of monoclinic β-Ga_2S_3 and has been exploited for spectral shifting in a Si solar cell resulting into an increase of the power conversion efficiency from 7.2% to 8.3%.
 [http://dx.doi.org/10.1063/1.4935633]

I. INTRODUCTION

Metal oxide (MO) NWs such as ZnO,[1] SnO_2,[2] In_2O_3,[3] Sn doped In_2O_3,[4] and Ga_2O_3[5] NWs have been used extensively for the fabrication of nanoscale electronic and optoelectronic devices such as nanowire solar cells, sensors, and photodetectors. In particular, Sn doped In_2O_3 NWs with metallic like conductivities and high transparency have been investigated in detail, while Sn doping of Ga_2O_3 has also been considered to enable its use in devices. Tetravalent Sn is a good doping candidate for Ga_2O_3 because it has an ionic radius of 0.69 Å which is close to that of octahedraly coordinated Ga i.e., 0.62 Å. Very recently, the resistivity of Sn doped Ga_2O_3 epitaxial layers grown by metal organic chemical vapour deposition on Ga_2O_3(001) was investigated by Du *et al.*,[6] who found that the resistivity changed over nine orders of magnitude from 10^7 to 10^{-1} Ω cm upon increasing the Sn content up to 10% and also observed a slight reduction in the energy band gap with increasing content of Sn attributed to the narrower band gap of SnO_2. Similarly, Orita *et al.*[7] prepared Sn doped β-Ga_2O_3 by pulsed laser deposition on glass and sapphire with a minimum resistivity of 1 Ω cm. The electrical conductivity of β-Ga_2O_3 has also been controlled over three orders of magnitude by Si doping.[8] In addition to epitaxial layers, Sn doped β-Ga_2O_3 and β-Ga_2O_3/SnO_2 NWs have been grown by the vapour-liquid-solid (VLS) method at 900 °C, using Ga:Sn alloys with 98:2 and 92:8 wt. % ratios as sources, but Sn exhibits low solubility in β-Ga_2O_3 and only small amounts of 0.5 at. % Sn have been shown to be incorporated successfully thereby improving the electrical conductivity.[9,10]

Besides doping, the surface passivation of MO NWs is also necessary to prevent fluctuations in their conductivity due to the adsorption and desorption of oxygen or water. This has been carried out on ZnO and SnO_2 NWs using polyimide and poly methyl methacrylate, respectively.[11,12] Sulphur passivation has been used to improve the properties of III-V NWs but not MO NWs. Recently, we investigated the sulphur passivation and conversion of SnO_2 into SnS_2 NWs,[13] while we have shown that the exposure of Sn doped In_2O_3 NWs to H_2S between 100 °C and 600 °C resulted in the formation of SnS_2/In_2O_3 NWs and the emergence of band edge photoluminescence (PL) emission at 3.4 eV corresponding to In_2O_3 which was not observed in the as-grown Sn doped In_2O_3 NWs.[14] Therefore, the sulphur passivation of MO NWs may be used to improve their properties but also obtain metal oxy-sulphide (MOxS) NWs with different electrical and optical properties similar to β-$In_2S_{3-3x}O_{3x}$. The latter has an optical band gap which was found to vary from 2.1 eV in pure β-In_2S_3 to 2.9 eV when it contained 8.5 at. % of oxygen and has been proposed as an alternative to CdS buffer layers in $CuIn_xGa_{1-x}Se_2$ solar cells.[15] Besides, the sulphur passivation of MO NWs is also useful for their incorporation in devices where they are subjected to various liquids containing S, Na_2S, e.g., in quantum dot sensitised solar cells (QDSSc). The promise and challenges of nanostructured solar cells have been recently described by Beard *et al.*[16] while it has been shown that the efficiency of solar cells may be improved by integrating a luminescent spectral conversion layer into the cell structure.[17] Evidence of spectral shifting in Si solar cells was recently shown using $CuInS_2$/ZnS core-shell QDs with red emission,[18] so the conversion of β-Ga_2O_3 to β-Ga_2S_3 NWs with red emission may be also beneficial for improving the performance of Si solar cells.

Hence we have undertaken an investigation into (a) the growth of Sn doped Ga_2O_3 NWs via the VLS mechanism over a broader range of compositions than what has been

[a)]Author to whom correspondence should be addressed. Electronic mail: zervos@ucy.ac.cy

considered previously and their structural, electrical, and optical properties and (b) the effect of post growth processing under H_2S between 300 °C and 900 °C and the use of the resultant β-Ga_2S_3/Ga_2O_3 NWs for spectral shifting in a Si solar cell. We find that the Sn doped β-Ga_2O_3 NWs with 1–2 at. % Sn exhibited broad PL with a maximum at 2.7 eV and had the smallest resistances consistent with the findings of Du *et al.*[6] Increasing the Sn content of the source, resulted into the formation of tetragonal rutile SnO_2 and a gradual suppression of the β-Ga_2O_3 phase, that was accompanied by a large increase in resistance but the PL did not change significantly. However, we observed a red shift of the PL from 2.7 eV to 1.8 eV upon post growth processing of the Sn doped Ga_2O_3 NWs containing only 1–2 at. % Sn under H_2S between 600 °C and 900 °C. The red emission is directly related to the formation of monoclinic β-Ga_2S_3 NWs and radiative transitions between deep donor to acceptor states which has not been observed previously in one dimensional Ga_2S_3 NWs. This has been exploited for spectral shifting in a Si solar cell resulting into an increase of the power conversion efficiency from 7.2% to 8.3%.

II. METHODS

Sn doped Ga_2O_3 NWs were grown using a low-pressure chemical vapour deposition (LPCVD) hot wall reactor consisting of a 1 in. quartz tube, capable of reaching 1100 °C which was fed from a manifold with four mass flow controllers connected to Ar, O_2, NH_3, and H_2. For the growth of the Sn doped Ga_2O_3 NWs, Sn (Aldrich, 2–14 Mesh, 99.9%) and Ga (Aldrich, 99.9%) were weighed with an accuracy of ± 1 mg. Square samples of Si(001) $\approx 7\,\text{mm} \times 7\,\text{mm}$ were cleaned sequentially in trichloroethylene, methanol, acetone, and isopropanol, rinsed with de-ionised water, dried with nitrogen, and coated with $\approx$1 nm Au. Following this, 0.2 g of Sn and Ga containing 1, 4 and 10, 20, 30, 40, 50, 60, 70, 80, and 90% wt. Sn were used as a source for the growth of the Sn doped Ga_2O_3 NWs and the 1 nm Au/Si(001) substrates were loaded in a boat which was positioned at the centre of the 1 in. tube. The latter was pumped down to 10^{-4} mbar and subsequently purged with 600 sccms of Ar for 10 min at 10^{-1} mbar, after which the temperature was increased up to 800 °C using a ramp rate of 30 °C/min while maintaining the same flow of Ar. Upon reaching 800 °C, a small flow of 10 sccms O_2 was added to the main flow of Ar in order to grow the Sn doped Ga_2O_3 NWs over 60 min, followed by cool down over 30 min without O_2. The morphology of the Sn doped Ga_2O_3 NWs was determined by scanning electron microscopy (SEM) while their crystal structure was determined by x-ray diffraction (XRD) using a Rigaku Miniflex. In addition, the Sn and Ga content were determined by energy dispersive X-ray analysis (EDX) using a Si detector with resolution of 100 eV and accelerating voltage of 20 kV. The actual % at. content of Sn and Ga in the Sn doped Ga_2O_3 NWs determined by EDX should not be confused with the % wt. of Ga or Sn used on the upstream side as a source for the growth of the Sn doped β-Ga_2O_3 NWs.

Steady state absorption-transmission spectra of the Sn doped Ga_2O_3 NWs, grown on fused silica for 10 min in order to maintain transparency, were obtained with a Perkin-Elmer UV-Vis spectrophotometer while the PL of the Sn doped Ga_2O_3 NWs on Si(001) was measured between 10 and 300 K using an excitation wavelength of 266 nm. The resistance of the Sn doped Ga_2O_3 NW networks that were grown on 5 mm $\times$ 10 mm fused silica for the purpose of applying large voltages were measured in a two terminal configuration similar to Ho and Chen[19] using Ag contacts. Furthermore, the Sn doped Ga_2O_3 NWs were exposed to 50 sccm H_2S between 300 °C and 900 °C for 60 min using a ramp rate of 10 °C/min in a different hot wall reactor capable of reaching 1500 °C and their morphology was inspected again by SEM while changes in their crystal structure were determined by XRD and the steady state absorption—transmission and PL were measured again between 10 and 300 K. Finally, the resultant β-Ga_2S_3/Ga_2O_3 NWs were deposited on the front surface of a Si solar cell which was fabricated by Al induced crystallization of an amorphous layer of Si resulting into simultaneous p-type doping, details of which are described elsewhere[20] and the I V characteristics were obtained in the dark but also under light.

III. RESULTS AND DISCUSSION

We have shown previously that the reaction of Ga with O_2 at 900 °C and 1 atm lead to the growth of β-Ga_2O_3 NWs on 1 nm Au/Si(001) with lengths up to $\approx$100 μm and diameters of $\approx$50 nm but the yield and uniformity over areas greater than 10 mm $\times$ 10 mm was not satisfactory. The β-Ga_2O_3 NWs had a monoclinic β-Ga_2O_3 crystal structure with lattice constants of a = 12.23 Å b = 3.04 Å, c = 5.80 Å, and $\beta = 103.7°$ belonging to the C_{2h}^3 C $2/m$ space group. The β-Ga_2O_3 NWs exhibited PL with a maximum at 520 nm or 2.4 eV, related to oxygen vacancies and states lying energetically in the upper half of the energy band gap of β-Ga_2O_3 as shown by ultrafast absorption-transmission spectroscopy.[21] Interestingly, these β-Ga_2O_3 NWs were fully converted into GaN NWs with a hexagonal wurtzite crystal structure under 250 sccm of NH_3 between 900 °C and 1000 °C, which also resulted into a gradual suppression and shift of the PL from 2.4 eV to 3.4 eV, corresponding to band edge emission from the GaN NWs.[22] We did not observe any residual or side emission at 520 nm or 2.4 eV left over from the original β-Ga_2O_3 NWs. Similar to the growth of β-Ga_2O_3 NWs, we have found that In_2O_3 NWs with lengths up to $\approx$1 μm and diameters of $\approx$50 nm could be obtained on 1 nm Au/Si(001) at 700 °C and 1 atm via the reaction of In and O_2 (Ref. 23) but the yield and uniformity was also limited to $\approx$10 mm $\times$ 10 mm. In contrast, a significantly higher yield and uniform distribution of Sn doped In_2O_3 NWs with lengths up to $\approx$100 μm and diameters of $\approx$50 nm were obtained by LPCVD on 1 nm Au/Si(001) over areas greater than 10 mm $\times$ 10 mm up to $\approx$100 mm away from the source of Sn and In at 800 °C and 1 mbar.[4] This is a direct consequence of the large vapor pressure of In and Sn at 10^{-1} mbar and 800 °C. The Sn doped In_2O_3 NWs grown via the VLS mechanism have a cubic bixbyite crystal structure, metallic like conductivities and exhibited PL at 2.4 eV while post growth processing under H_2S up to 400 °C resulted into

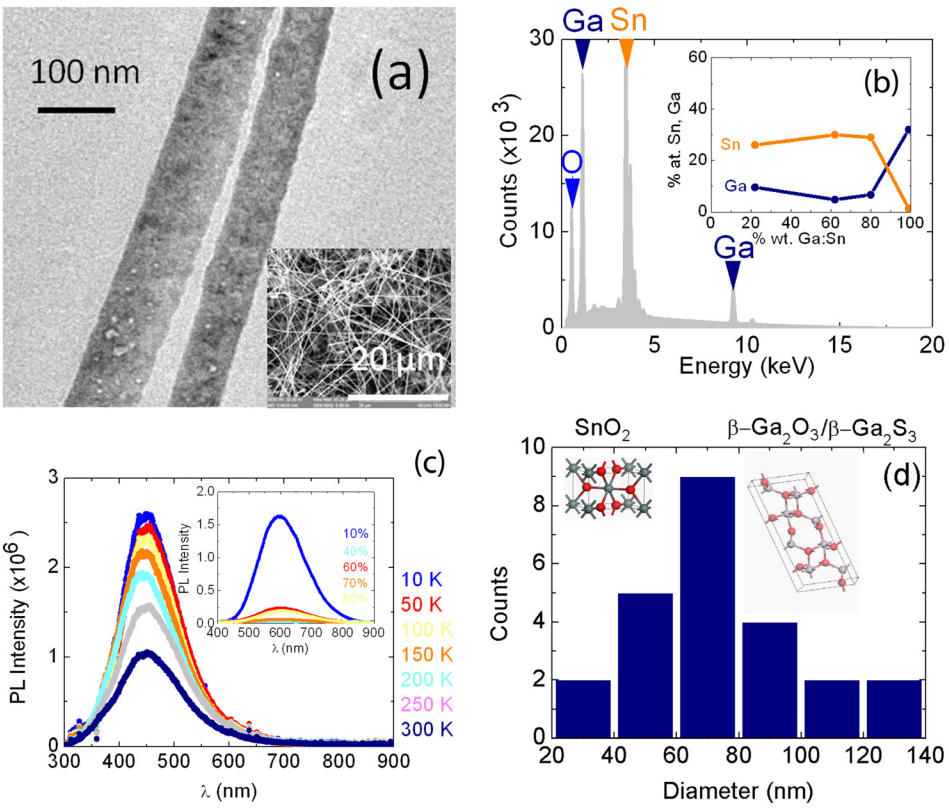

FIG. 1. (a) TEM image of the Sn doped β-Ga_2O_3 NWs grown on 1 nm Au/Si(001) at 800 °C and 1 mbar with ≈1 at. % Sn; inset shows SEM image of Sn doped β-Ga_2O_3 NW network (b) typical EDX spectrum of SnO_2/β-Ga_2O_3 NWs containing ≈25 ± 3 at. % Sn; inset shows variation of the at. % Sn and Ga in the Sn doped β-Ga_2O_3 NWs versus % wt. of Ga: Sn used as a source for their growth (c) temperature dependence of the PL from Sn doped Ga_2O_3 NWs with 1–2 at. % Sn between 10 and 300 K; inset shows the PL of the SnO_2/Ga_2O_3 NWs obtained using more than 10% Sn (d) histogram of diameters; insets show the stick and ball crystal structures of SnO_2 and Ga_2S_3/Ga_2O_3.

the emergence of PL at 3.5 eV, which is close to band edge emission of cubic In_2O_3.[14]

Here, we have grown Sn doped β-Ga_2O_3 NWs on 1 nm Au/Si(001) using exactly the same growth conditions used for Sn doped In_2O_3 NWs and obtained a high yield, uniform distribution of β-Ga_2O_3 NWs over large areas, greater than 10 mm × 10 mm, which is important for their growth on Si wafer solar cells. A typical SEM and TEM image is shown in Fig. 1(a) from which we find that the Sn doped β-Ga_2O_3 NWs have lengths of ≈100 μm and average diameters of 70 nm as shown in Fig. 1(d). The Sn doped β-Ga_2O_3 NWs have the monoclinic crystal structure of β-Ga_2O_3 as shown by the XRD in Fig. 2, but we also detected peaks corresponding to the tetragonal rutile crystal structure of SnO_2 above 4 % wt. Sn, which was accompanied by a gradual suppression of the monoclinic β-Ga_2O_3 crystal structure. Hence, we have the formation of two distinct phases, i.e., in essence SnO_2/β-Ga_2O_3 NWs. Note that SnO_2 has a tetragonal rutile crystal structure and belongs to the $P4_2/mnm$ No.136 space group with lattice constants of a = 4.737 Å and c = 3.185 Å. A stick and ball model of the tetragonal rutile crystal structure as well as the monoclinic β-Ga_2O_3 is shown as an inset in Fig. 1(d). These findings are similar to the case of Sn doped In_2O_3 NWs, where we have shown that it is possible to tune the crystal structure and composition from pure SnO_2 with a tetragonal rutile crystal structure to pure cubic bixbyite In_2O_3 simply by varying the ratio of Sn to In of the metal source which also results into a mixture of two phases in between, i.e., SnO_2/In_2O_3 NWs.[4] A typical EDX spectrum of the SnO_2/β-Ga_2O_3 NWs consisting of tetragonal rutile SnO_2 and monoclinic β-Ga_2O_3 is shown in Fig. 1(b) where one may clearly observe the peaks belonging to Sn and Ga. We find that the β-Ga_2O_3 NWs obtained using 1–4 wt. % Sn actually contain 1–2 at. % Sn as shown by the inset in Fig. 1(b). This is due to the limited solubility of Sn in β-Ga_2O_3 similar to that of Sn doped In_2O_3. All of the SnO_2/β-Ga_2O_3 NWs obtained using 10–80 wt. % Sn consist of 30 at. %. Sn and 10 at.% Ga suggesting that the tetragonal rutile SnO_2 phase is dominant compared to the monoclinic

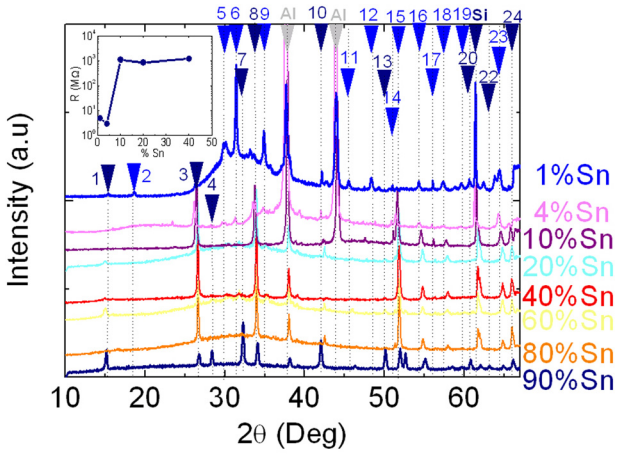

FIG. 2. XRD traces of Sn doped β-Ga_2O_3 NWs as grown on 1 nm Au/Si(001) at 800 °C and 1 mbar obtained with 1%, 4%, 10%, 20%, 40%, 60%, 80, and 90% Sn. The peaks have been labeled using arrows for clarity, in ascending order with increasing angle and correspond to 1 ▶ SnO_2, 2 ▶ β-Ga_2O_3, 3 ▶ (110) SnO_2, 4 ▶ SnO_2, 5 ▶ (400) β-Ga_2O_3, 6 ▶ (002) β-Ga_2O_3, 7 ▶ SnO_2, 8 ▶ (101) SnO_2, 9 ▶ (111) β-Ga_2O_3, 10 ▶ (-112) β-Ga_2O_3, 11 ▶ (110) β-Ga_2O_3, 12 ▶ β-Ga_2O_3, 13 ▶ (402) β-Ga_2O_3,14 ▶ (120) β-Ga_2O_3, 15 ▶ (211) SnO_2, 16 ▶ (220) SnO_2, 17 ▶ (-113) β-Ga_2O_3, 18 ▶ (002) SnO_2, 19 ▶ (113) β-Ga_2O_3, 20 ▶ SnO_2, 21 ▶ Si(001), 22 ▶ SnO_2 23 ▶ (301) SnO_2, 24 ▶ SnO_2; inset shows variation of resistance of the Sn doped β-Ga_2O_3 NWs at 300 K versus % wt. Sn.

β-Ga_2O_3. These SnO_2/β-Ga_2O_3 NWs exhibited broad PL with a maximum at 2.6 eV as shown as an inset in Fig. 1(c) which is similar to the PL of the β-Ga_2O_3 NWs grown at 900 °C and 1 atm that had a maximum at 2.5 eV. Note that β-Ga_2O_3 has a direct energy gap of 4.7 eV, while SnO_2 has a direct energy band gap of 3.7 eV but the even-parity symmetry of the conduction-band minimum and valence-band maximum states prohibits band-edge radiative transitions. The broad PL of the SnO_2/β-Ga_2O_3 NWs is attributed to defect states lying energetically in the upper half of the energy band gap of SnO_2 and Ga_2O_3. However, we find that the Sn doped Ga_2O_3 NWs containing 1–2 at. % Sn exhibited PL at 450 nm, shown in Fig. 1(c), which is slightly blue shifted. This is attributed to a suppression of the tetragonal rutile SnO_2 and related states similar to what we have also found in Sn doped In_2O_3 NWs. Moreover, this is consistent with the findings of Du *et al.*[6] who observed a slight reduction in the optical band gap with increasing Sn content attributed to the narrower band gap of SnO_2 although the even-parity symmetry of the conduction-band minimum and valence-band maximum states prohibits band-edge radiative transitions in bulk SnO_2.

The Sn doped β-Ga_2O_3 NWs assemblies do not have metallic like conductivities like Sn doped In_2O_3 NWs. It is well known that β-Ga_2O_3 has n-type conductivity due to oxygen vacancies and/or Ga interstitials, but the conductivity is poor at room temperature because of its large band gap which is equal to 4.7 eV.[24] This has hindered its exploitation in electronic and optoelectronic devices and consequently doping is required. We have measured the resistances of the Sn doped β-Ga_2O_3 NW networks grown on fused silica in a two terminal configuration using Ag contacts and found that the resistances reached a minimum around 1–2 at. % Sn after which we observed a rapid increase in their resistance as shown by the inset in Fig. 2. This may be understood as follows. When the vapor pressure of Sn is small relative to that of Ga we have the formation of Sn doped β-Ga_2O_3 NWs whose resistances, initially fall with increasing content and the incorporation of Sn into the β-Ga_2O_3 NWs, consistent with the findings of Du *et al.*[6] However, when the vapor pressure of Sn is larger than that of Ga it leads to the preferential formation of SnO_2 which have large resistances due to the small carrier density which is of the order of $\approx 10^{16}\,cm^{-3}$ as we have shown previously by THz conductivity spectroscopy.[2] These trends are in agreement with Du *et al.*[6] who found that the resistivity changed over nine orders of magnitude from $10^7\,\Omega\,cm$ to $10^{-1}\,\Omega\,cm$ upon increasing the Sn content from 0% to 10%. Evidently, the Sn content is critical and care is required to obtain Sn doped β-Ga_2O_3 NWs with reasonable conductivities and resistances for their exploitation in devices.

All of the SnO_2/β-Ga_2O_3 NWs, containing 30 at. %. Sn and 10 at. % Ga with a dominant SnO_2 phase were processed under H_2S at 500 °C but we did not observe any monoclinic or cubic Ga_2S_3 or hexagonal GaS in the XRD spectra shown in Fig. 3. Instead, we observed the existence of SnS_2, monoclinic β-Ga_2O_3, and the tetragonal rutile crystal structure of SnO_2. In other words, the SnO_2/Ga_2O_3 NWs processed under H_2S consist of three different phases, i.e., SnS_2, SnO_2, and

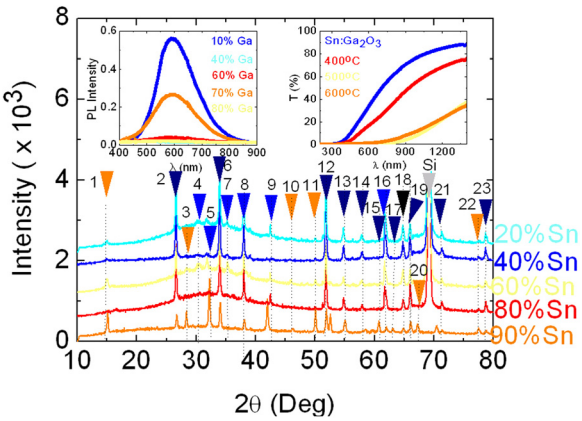

FIG. 3. XRD spectra of the Sn doped β-Ga_2O_3 NWs following post growth processing under 50 sccm of H_2S at 500 °C for 60 min. The peaks are labeled in ascending order with increasing angle as follows: 1 ▶ (001) SnS_2, 2 ▶ (110) SnO_2, 3 ▶ (100) SnS_2, 4 ▶ (400) β-Ga_2O_3, 5 ▶ (002) β-Ga_2O_3, 6 ▶ (101) SnO_2, 7 ▶ (111) β-Ga_2O_3, 8 ▶ Al, 9 ▶ (-112) β-Ga_2O_3, 10 ▶ (003) SnS_2, 11 ▶ (110) SnS_2, 12 ▶ (211) SnO_2, 13 ▶ (220) SnO_2, 14 ▶ (002) SnO_2, 15 ▶ (310) SnO_2, 16 ▶ Si(001), 17 ▶ (020) SnO_2, 18 ▶ (112) SnO_2, 19 ▶ (301) SnO_2, 20 ▶ (202) SnS_2, 21 ▶ (202) SnO_2, 22 ▶ (203) SnS_2, 23 ▶ (321) SnO_2; left inset shows the PL of SnO_2/Ga_2O_3 NWs after processing under H_2S at 500 °C; right inset shows steady state transmission spectrum of the Sn doped β-Ga_2O_3 NWs with 1%–2% at Sn as-grown on fused silica before and after post growth processing under H_2S at 400 °C, 500 °C, and 600 °C.

β-Ga_2O_3 and exhibited broad PL at ≈600 nm or 2.5 eV as shown in Fig. 3 which is more or less identical to that of the as-grown SnO_2/Ga_2O_3 NWs shown in Fig. 1. The broad PL is related to defect states in the SnO_2 and β-Ga_2O_3 but also possibly SnS_2 which is an indirect band gap semiconductor known to exhibit defect emission at ≈2.0 eV.

In contrast, the Sn doped Ga_2O_3 NWs, containing only 1 to 2 at. % Sn and dominant β-Ga_2O_3 phase, that were processed under H_2S at 700 °C–900 °C exhibited a red-shift of the PL from 2.7 eV to 1.8 eV, as shown in the inset of Fig. 4, which is directly related to the emergence of monoclinic Ga_2S_3 as shown by the XRD traces of Fig. 4. The peaks of Ga_2S_3 are in good agreement with those observed from layered Ga_2S_3[25] but before elaborating further, we ought to mention that Ga_2S_3 is III-VI semiconductor which can have the monoclinic, hexagonal, or cubic crystal structure. Among these, the most stable crystal structure is monoclinic of Ga_2S_3 with lattice constants of β-Ga_2S_3 are a = 11.11 Å, b = 9.58 Å and c = 6.4 Å, β= 141.15°. Monoclinic β-Ga_2S_3 has a direct energy gap of 3.4 eV but contains many vacancies in its Ga sub lattice and consequently exhibits red emission due to deep donor to acceptor transitions related to S and Ga vacancies. Despite the fact that one third of the Ga sub-lattice sites are not occupied, Ga_2S_3 has been investigated for light-emitting diodes and photovoltaic devices, while recently it was shown that Ga_2S_3 has a large second-harmonic generation efficiency ideally suited for nonlinear optics.[26] However so far, one dimensional GaS or Ga_2S_3 nanotubes have shown PL only between 450 and 600 nm. For instance, GaS NWs obtained by the vapor solid (VS) method exhibited PL between 550 and 600 nm while Hu *et al.*[27] obtained GaS NTs with PL at 450 nm. Hexagonal GaS, has a direct energy band gap of 3.05 eV and an indirect

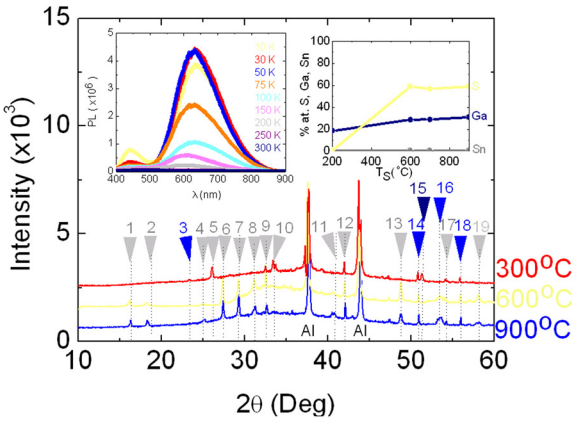

FIG. 4. XRD spectra of the Sn doped Ga_2O_3 NWs containing 1–2 at. % Sn that were processed under H_2S at 300 °C, 600 °C, and 900 °C. The peaks are labeled for clarity, in ascending numerical order with increasing angle as follows: 1 ▶ (001) Ga_2S_3, 2 ▶ (-201/-110) Ga_2S_3, 3 ▶(012) Ga_2O_3, 4 ▶ (300) Ga_2S_3, 5 ▶ (200) Ga_2S_3, 6 ▶ (-312) Ga_2S_3, 7 ▶ (101) Ga_2S_3, 8 ▶ (002) Ga_2S_3, 9 ▶ (-311) Ga_2S_3, 10 ▶ (-111) Ga_2S_3, 11 ▶ (-314) Ga_2S_3, 12 ▶ (-112) Ga_2S_3, 13 ▶ (-332) Ga_2S_3, 14 ▶ (-403) Ga_2O_3, 15 ▶ (211) SnO_2, 16 ▶ (203) Ga_2O_3, 17 ▶ (-315/023/311) Ga_2S_3, 18 ▶ (-113) β-Ga_2O_3, 19 ▶ (311) Ga_2S_3. The left inset shows the PL of Sn doped Ga_2O_3 NWs containing 1–2 at. % between 10 and 300 K after processing under H_2S at 900 °C; right inset shows the variation of % at. Sn, Ga, and S in the Sn doped β-Ga_2O_3 NWs with small content of Sn processed under H_2S between 200 °C and 900 °C.

energy gap of 2.5 eV and Sinha *et al.*[28] observed PL from GaS NWs at 450 nm. On the other hand, Ga_2S_3 has an energy gap of 3.4 eV and Liu *et al.*[25] observed PL from layered structures of Ga_2S_3 with a maximum around 1.6 eV, which, however, was broad and extended to 3.0 eV.

Evidently, the red emission of the Sn doped Ga_2O_3 NWs with 1%–2% Sn observed at 680 nm or 1.8 eV is directly related to the formation of Ga_2S_3 not Sn and is found to persist down to 10 K, while it is also stronger than the blue emission at 2.7 eV, as shown in Fig. 4. The steady state transmission spectra through β-Ga_2O_3 NWs, that were grown on fused silica before and after exposure to H_2S at 400 °C, 500 °C, and 600 °C, are shown as an inset in Fig. 3 and suggest a decrease in the optical band gap and overall transmission coefficient consistent with the formation of β-Ga_2S_3. The red emission obtained from the β-Ga_2O_3/Ga_2S_3 NWs could be used for the fabrication of sensors or solar cells since evidence of spectral shifting resulting into the improvement of efficiency in Si solar cells has been shown to be possible using $CuInS_2$/ZnS core-shell quantum dots with red emission.[18] We have fabricated a p^+n junction solar cell where the p^+ layer was formed by Al induced crystallization of an amorphous layer of Si, resulting into simultaneous p-type doping of the layer, details of which are described elsewhere.[20] The amorphous Si layer was 20 nm thick and the Al layer 10 nm thick, while the solar cell surface area was 1 cm^2, as shown in Fig. 5. The bare solar cell without the β-Ga_2O_3/Ga_2S_3 NWs had an open circuit voltage $V_{OC} = 0.42$ V, short circuit current density $J_{SC} = 27.2$ mA/cm^2, and fill factor 63%, resulting in a conversion efficiency of $\eta = 7.2\%$. After deposition of the β-Ga_2O_3/Ga_2S_3 NWs by drop casting, the device exhibited a short circuit current $J_{SC} = 32.37$ mA/cm^2, Voc = 0.42 V, and fill factor of 61%,

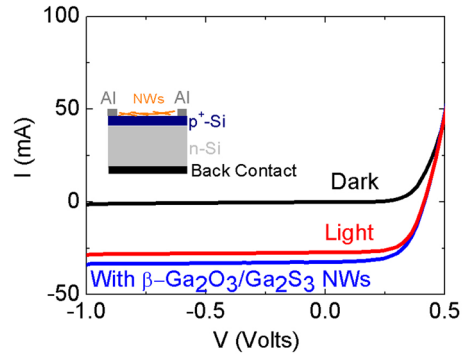

FIG. 5. I V characteristics of a Si solar cell in the dark and under one sun, before and after the transfer of β-Ga_2O_3/Ga_2S_3 NWs; inset shows schematic diagram of device.

with the efficiency η increasing from 7.2% to 8.3%, which corresponds to an increase of ≈14%. This is attributed to spectral shifting and a reduction in the reflection coefficient.[17] Further improvements may be attained by the growth of an ordered array of Sn doped β-Ga_2O_3 NWs on the surface of Si while the red emission of the β-Ga_2O_3/Ga_2S_3 NWs could also be utilised in quantum dot sensitised solar cells.

IV. CONCLUSION

Sn doped Ga_2O_3 NWs have been grown via the VLS mechanism at 800 °C over a broad range of compositions than what has been considered previously. The Sn doped Ga_2O_3 NWs exhibited PL between 450 and 600 nm and had minimum resistances for 1–2 at. % Sn above which we observed the formation of SnO_2 which also lead to an increase in the resistance by more than three orders of magnitude. A strong red shift of the PL from 2.7 eV to 1.8 eV nm occurred after post growth processing the Sn doped Ga_2O_3 NWs with 1–2 at. % Sn under H_2S between 700 °C and 900 °C. The red emission of β-Ga_2S_3 is due to deep donor to acceptor transitions related to S and Ga vacancies. We show that the red emission of the β-Ga_2O_3/β-Ga_2S_3 NWs randomly deposited on the surface of a Si solar cell can be used for spectral shifting resulting into an increase of the power conversion efficiency from 7.2% to 8.3% corresponding to an increase of ≈14%.

[1] M. Law, L. E. Greene, J. C. Johnson, R. Saykally, and P. Yang, Nat. Mater. **4**, 455 (2005).
[2] D. Tsokkou, A. Othonos, and M. Zervos, Appl. Phys. Lett. **100**, 133101 (2012).
[3] D. Tsokou, M. Zervos, and A. Othonos, J. Appl. Phys. **106**, 084307 (2009).
[4] M. Zervos, C. Mihailescu *et al.*, Appl. Phys. Lett. Mater. **2**, 056104 (2014).
[5] I. Lopez, A. Castaldini, A. Cavallini, and E. Nogales, J. Phys. D: Appl. Phys. **47**, 415101 (2014).
[6] X. Du, Z. Li, C. Luan, W. Wang, M. Wang, and X. Feng, J. Mater. Sci. **50**, 3252 (2015).
[7] M. Orita, H. Ohta, M. Hirano *et al.*, Appl. Phys. Lett. **77**, 4166 (2000).
[8] E. G. Villora, K. Shimamura, Y. Yoshikawa *et al.*, Appl. Phys. Lett. **92**, 202120 (2008).
[9] L. Mazeina, Y. Picard, S. Maximenko, and F. Perkins, Cryst. Growth Des. **9**, 4471 (2009).
[10] S. Maximenko, L. Mazeina, Y. N. Picard, and J. A. Freitas, Nano Lett. **9**, 3245 (2009).

[11]J. Huh, M. K. Joo, D. Jang, J. H. Lee, and G. T. Kim, J. Mater. Chem. **22**, 24012 (2012).
[12]W. I. Park, J. S. Kim, G. C. Yi, M. H. Bae, and H. J. Lee, Appl. Phys. Lett. **85**, 5052 (2004).
[13]M. Zervos, C. Mihailescu, A. Othonos, J. Giapintzakis *et al*., Mater. Sci. Eng., B. **198**, 10 (2015).
[14]M. Zervos, C. Mihailescu, G. Giapintzakis, and A. Othonos, Nano Res. Lett. **10**, 307 (2015).
[15]N. Barreau, S. Marsillac, D. Albertini, and J. Bernede, Thin Solid Films **403–404**, 331 (2002).
[16]M. C. Beard, J. M. Luther, and A. J. Nozik, Nat. Nanotechnol. **9**, 951 (2014).
[17]O. M. ten Kate, M. de Jong, H. T. Hintzen, and E. van der Kolk, J. Appl. Phys. **114**, 084502 (2013).
[18]S. Gardelis and A. G. Nassiopoulou, Appl. Phys Lett. **104**, 183902 (2014).
[19]C. H. Ho and H. H. Chen, Sci. Rep. **4**, 6143 (2014).
[20]S. Gardelis, A. G. Nassiopoulou, N. Vouroutzis, and N. Frangis, Appl. Phys. Lett. **103**, 241114 (2013).
[21]A. Othonos, M. Zervos, and C. Christofides, J. Appl. Phys. **108**, 124302 (2010).
[22]A. Othonos, M. Zervos, and C. Christofides, J. Appl. Phys. **108**, 124319 (2010).
[23]P. Papageorgiou, M. Zervos, and A. Othonos, Nanoscale Research Letters **6**, 311 (2011).
[24]N. Ueda, H. Hosono, R. Waseda *et al*., Appl. Phys. Lett. **70**, 3561 (1997).
[25]H. Liu, K. Antwi *et al*., ACS Appl. Mater. Interfaces **6**, 3501 (2014).
[26]M. Zhang, X. Jiang, L. Zhou, and G. Guo, J. Mater. Chem. C **1**, 4754 (2013).
[27]P. Hu, Y. Liu, L. Fu, L. Cao, and D. Zhu, Appl. Phys. A **80**, 1413 (2005).
[28]G. Sinha, S. Panda, A. Datta, P. Chavan *et al*., ACS Appl. Mater. Interfaces **3**, 2130 (2011).